

# Constraints on a Light WIMP from the Isotropic Diffuse Gamma-Ray Emission

Chiara Arina\* and Michel H.G. Tytgat†

*Service de Physique Théorique, Université Libre de Bruxelles,  
CP225, Bld du Triomphe, 1050 Brussels, Belgium*

Motivated by the measurements reported by direct detection experiments, most notably DAMA, CDMS-II, CoGeNT and Xenon10/100, we extend to lower masses,  $M_{DM} \sim \text{few GeV}$ , the constraints on the annihilation of dark matter from the Fermi-LAT data on the isotropic gamma-ray diffuse emission. Depending on the assumption made on the distribution of dark matter halos in the universe, we show that interesting constraints may be set on a light WIMP, *i.e.* a candidate with an annihilation cross-section in the pbarn range. We consider in particular two candidates: a Dirac fermion singlet interacting through a  $Z'$  boson, and a scalar singlet  $S$  interacting through the Higgs portal. In the latter case, a one-to-one correspondence between its annihilation cross-section and its spin-independent elastic scattering cross-section permits to express the constraints from the Fermi-LAT data in the direct detection exclusion plot,  $\sigma_n^0 - M_{DM}$ . Depending on the astrophysics, we show that it may be possible to exclude a scalar dark matter candidate at 95% confidence level.

## I. INTRODUCTION

The cosmological data show evidence of dark matter (DM) [1], but the nature of the DM particle, if any, is still unknown. Recently, some interest has been taken in a light WIMP<sup>1</sup>, with mass  $M_{DM} \lesssim 10 - 15 \text{ GeV}$ . This is motivated by the modulation observed by the DAMA/LIBRA and DAMA/NaI experiments [2], the excess of events at low recoil energies measured by CoGeNT [3], and an anomaly reported by the CRESST collaboration at conferences [4]. If interpreted in terms of the elastic scattering of a DM particle, these experiments all point to a candidate with a mass in the few GeV range, and a spin-independent (SI) elastic cross-section  $\sigma_n^0 \mathcal{O}(10^{-40}) \text{ cm}^2$  [5–10]. Whether these results, to which we will loosely refer as CoGeNT-DAMA, are due to dark matter or to a more mundane sort of background is a matter of debate (see e.g. [11–13]). Furthermore, other direct detection experiments have set exclusion limits that may exclude part or whole regions of the parameter space favoured by CoGeNT and/or DAMA (see for instance [7] and [14]). Most relevant for the low mass region,  $M_{DM} \lesssim 15 \text{ GeV}$ , are the CDMS-Si [15], CDMS-II [16], Xenon10 [17, 18] and Xenon100 [19] exclusion limits. However, it is quite delicate to set robust exclusion limits in the low mass region, which in the direct detection experiments corresponds to small recoil energies<sup>2</sup>, and it may pay to look for alternative ways to constrain a light WIMP.

A possibility is to consider signatures that are specific to DM, like neutrinos from the Sun. Indeed a light WIMP (at least those relevant for CoGeNT-DAMA) have a large scattering cross-section on matter, and thus may be efficiently captured in the Sun. Their subsequent annihilation at the centre of the Sun may release a flux of neutrinos, which may be constrained with Super-Kamionkande data [6, 8, 25–27]. Another interesting possibility is missing energy at colliders, and limits set by the Tevatron and the LHC may, depending on the assumed properties of the light WIMP, be competitive with direct searches [28, 29].

Although more prone to astrophysical uncertainties, the flux of gamma-rays from the universe may also put relevant constraints on a light WIMP. Although the number of photons produced in the annihilation of a pair of DM particles is small, typically  $\mathcal{O}(10)$  for a 10 GeV candidate annihilating into  $b\bar{b}$  quarks, it is more than compensated by the  $1/M_{DM}^2$  dependence of the gamma-ray flux, for fixed energy density  $\rho_{DM}$ . Explicit statements regarding a light WIMP have been given in [8, 30, 31], focusing on the flux from the centre of the Galaxy, and in [8] and also [9] for dwarf galaxies. In the present article, we consider the constraints that may be set on a light WIMP based on the first-year Fermi-LAT data on the spectrum of isotropic diffuse gamma-ray emission [32]. That this measurement may

---

\*Electronic address: carina@ulb.ac.be

†Electronic address: mtytgat@ulb.ac.be

<sup>1</sup> By a WIMP we mean a cold dark matter candidate, with an annihilation cross-section of the order of 1 pbarn, so that its relic abundance may be fixed by the standard thermal freeze-out mechanism. This potentially includes many candidates, whose interactions might have nothing (or little) to do with weak interactions.

<sup>2</sup> The exclusion limits may be very sensitive to parameters which are poorly constrained, see for instance the discussion revolving around the scintillation efficiency in LXe experiments [9, 20–24].

be relevant for a light WIMP is no surprise, since current analysis show the common trend that the constraints on the annihilation cross-section get stronger for lower DM masses [33–36]. Also, depending on assumptions made on the DM distribution as a function of redshift, the limits may have a dent in regions of annihilation cross-section which are expected to be characteristic of a thermal relic,  $\langle \sigma v \rangle_{ann} \sim 3 \cdot 10^{-26} \text{ cm}^3\text{s}^{-1}$ . In particular, although we use a different approach to the calculation of the boost from extragalactic DM halos, our results are consistent with those of [36], where they overlap, and of [34], which also shows limits relevant for a light WIMP. However, our emphasis is more on the constraints on the CoGeNT-DAMA regions and on related particle physics models.

The plan of our article is as follows. In section II, we briefly expose our hypothesis regarding the isotropic diffuse gamma-ray emission. As in [36], we will suppose that the contribution from dark matter annihilation within the halo of our galaxy (and possible subhalos within) is negligible, and so, that the dominant contribution is to the isotropic gamma-ray background radiation (IGRB), which we will compute following the Press-Schechter formalism. In section III, we discuss the exclusion limits in general terms, and compare our results with other approaches. In section IV, we compare the outcome of our calculations for two minimal, toy models of dark matter which have been shown to be consistent with both CoGeNT-DAMA and WMAP, but have distinctive characteristics: a scalar candidate interacting through the Higgs portal, thus with “Higgs-like” couplings to ordinary matter, and a Dirac fermion interacting through a  $Z'$ , hence with “Z-like” couplings. Our main conclusions are given in Figures 6 and 7 for the scalar, and Figure 8 for the Dirac fermion.

## II. THE ISOTROPIC EXTRAGALACTIC GAMMA-RAY FLUX

In this section we summarize the formalism we have used to compute the extragalactic contribution to the gamma-ray from dark matter annihilation. We follow the approach of [37] and compare the result to other approaches in the next section.

To begin with, we will work with the hypothesis that the contribution of dark matter annihilation within the halo of our galaxy to the diffuse isotropic gamma-ray emission is small compared with the extragalactic component, or IGRB, following the approach of [36], to which we refer for future discussions on this point.

The flux of gamma-ray today (in units of  $\text{GeV}^{-1}\text{cm}^{-2}\text{s}^{-1}\text{sr}^{-1}$ ) from DM annihilation at any redshift  $z$  is then given by [38]<sup>3</sup>

$$\frac{d\Phi_\gamma}{dE} = \frac{c \langle \sigma v \rangle_{ann}}{4\pi 2M_{DM}^2} \int_0^\infty dz' \frac{1}{H(z')(1+z')^4} \frac{dN_\gamma}{dE'} \mathcal{B}^2(z') e^{-\tau(E',0,z')}. \quad (1)$$

In this equation  $H(z)(1+z) = H_0 h(z)(1+z)$  sets the relation between redshift interval and the proper distance interval, with  $h(z) = \sqrt{\Omega_M(1+z)^3 + \Omega_\Lambda}$ . For the cosmological parameters today we use the central value from the WMAP-7yrs measurements [1]:  $H_0 = 70.4 \text{ km/s/Mpc}$ ,  $\Omega_M = 0.227$ ,  $\Omega_b = 0.0456$  and  $\Omega_\Lambda = 0.728$ . A factor of  $(1+z)^{-3}$  accounts for the dilution of the number density of photons from expansion. Finally  $E' = E(1+z')$  is the energy of the photon at redshift  $z'$  for an energy  $E$  observed today. The factor  $dN_\gamma/dE'$  is the spectrum of gamma-rays produced in the annihilation of a pair of DM particle, at a rate given by  $\langle \sigma v \rangle_{ann}$ , and depends on the particle physics candidate. The function  $\mathcal{B}(z)$  takes into account the density profile of dark matter at a given redshift  $z$  and will be presented in Section II B. Finally the parameter  $\tau(E', z, z')$  is the optical depth (of a gamma-ray emitted at  $z'$  at energy  $E'$  and observed at  $z$ ), which takes into account the absorption that may occur on the path of a gamma-ray. For the case of a light WIMP ( $M_{DM} \lesssim 10 - 15 \text{ GeV}$ ), and focusing on the Fermi-LAT window, which has measured the isotropic flux between 200 MeV and 100 GeV, the universe is essentially transparent. This is an interesting simplification as it removes one source of uncertainty on the calculated gamma-ray flux, so we discuss this aspect in some details in the following section.

---

<sup>3</sup> The factor of 1/2 is for a self-conjugate DM candidate. In the case of a Dirac fermion which we will also consider, there is an extra 1/2 factor [38].

### A. Optical depth

For increasing energy, the dominant processes that may affect the propagation of a gamma-ray between redshift  $z$  and today are (see, for instance, [39])

Photoionization	$\gamma + H(He, He^+) \rightarrow e^- + H^+(He^+, He^{++}),$	(2)
Compton Scattering	$\gamma + e^- \rightarrow \gamma + e^-,$	(3)
$e^+e^-$ pair production on matter	$\gamma + A \rightarrow A + e^+ + e^-,$	(4)
Photon – photon scattering	$\gamma + \gamma_{\text{Bckgrd}} \rightarrow \gamma + \gamma,$	(5)
$e^+e^-$ pair production	$\gamma + \gamma_{\text{Bckgrd}} \rightarrow e^+ + e^-.$	(6)

To compute the processes (2) and (4) we have used the approach of [39], for Compton scattering we refer to [40], to [41] for pair production on a background photon and, finally to [42] for the photon-photon scattering contribution.

The results of our calculations are summarized in Figure 1, and they are in agreement with, for instance, [35]. There we show, in function of the observed energy today (dotted at  $z = 0$ ), the redshift  $1 + z'$  at which the optical depth was  $\tau(1 + z') = 1$ , such that the universe may be considered to be optically thin (transparent) at lower redshifts. The red (gray) region corresponds to the energy window of Fermi-LAT, which shows that only the (4-6) processes are relevant (see also [35]). The triangular region (in blue in the plot) within the Fermi-LAT window gives the allowed redshifts at emission in function of energy for a candidate with mass  $M_{DM} \lesssim 20$ . The fact that  $\tau(1 + z') \ll 1$  within the triangular means that the universe is optically thin for these gamma-rays. However, we show in the plot only the effect from scattering or pair creation on the photons from the CMB, as is relevant for large redshifts, but, at lower redshifts,  $z \lesssim 6 - 10$ , we should also take into account the ultraviolet (UV) photons produced by the formation of the first stars (an effect not shown in Figure 1). Unlike the CMB, there is much uncertainty regarding the distribution and spectrum of this extra background light. Here we follow [35] and also [43] and [44], where the possible impact of the low  $z$  UV background is discussed. In [35], three models for the UV background are considered. A glance at Figure 3 in Ref. [35] reveals that, for the case of a so-called realistic photon background, the effect is not relevant for a light WIMP. A similar conclusion may be drawn from the plots in Figure 11 of [43], which shown that absorption due

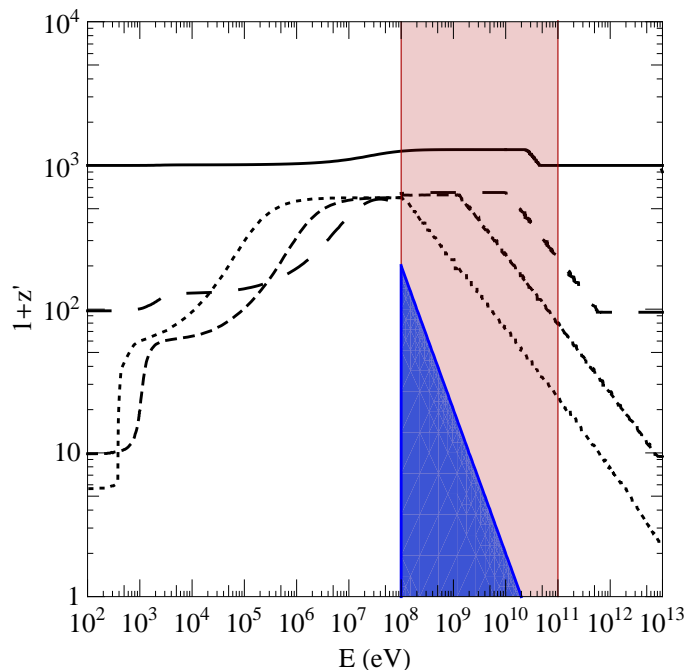


Figure 1: Contour plot of the optical depth with  $\tau(E', z, z') = 1$ , where  $E'/(1 + z') = E/(1 + z)$ . Here  $E$  is the energy observed at redshift  $z$ , so that  $E'$  is the emission energy at redshift  $z'$ . The different lines corresponding to the different observers. For each, they give the maximal possible redshift at emission:  $z = 0$  dotted line,  $z = 10$  dashed curve,  $z = 100$  long dashed line and  $z = 1000$  solid line. The red (gray) region denotes the Fermi-LAT measured energy range. The triangular region gives the relevant (for observations today) redshifts for a DM candidate of mass  $M_{DM} = 20$  GeV.

to UV photons is negligible within the range relevant for a light WIMP within the Fermi-LAT window. Absorption due to UV photons is more important according to the somewhat older model of [44], but, keeping in mind the fact that spectrum of photon produced by a, say, 20 GeV candidate typically peak at 1 GeV, we may safely conclude from this reference that absorption is essentially negligible, even in the most pessimistic scenario, if we concentrate on a light WIMP and the Fermi-LAT data. Thus, in the calculation of the gamma-ray flux, the only relevant astrophysical uncertainty is the distribution of dark matter halos as a function of redshift, which we now discuss.

## B. Enhancement factor from structure formation

To compute the extragalactic contribution to the gamma-ray flux from dark matter annihilation, we need the distribution of dark matter halos as a function of redshift. There are different approaches to this complicated problem. Needless to say, this will be the main source of uncertainty on our results. Here we found convenient to follow a standard, semi-analytical approach based on the Press-Schechter formula. In particular we follow the notation of [37], which is itself based on [45]. One should bare in mind that different approaches may give substantially different results. For a review on halo models and structure formation we refer to [46, 47].

As the universe expands, the initially small perturbations in the dark matter distribution evolve in a non-linear way into a complex network of structures made of dark matter halos of various scales. In the  $\Lambda$ CDM model for structure formation, dark matter halos are assumed to form hierarchically bottom-up, with small structures merging into larger halos, in a self-similar pattern. Under these hypotheses, the Press-Schechter [48] empirical formula gives an analytical expression for the abundance of dark matter halos of mass  $M$  at a given redshift  $z$ , on the basis of the predictions of linear perturbation theory for the power spectrum of perturbations:

$$\frac{dn}{dM}(z, M) = \sqrt{\frac{2}{\pi}} \frac{\rho_c \Omega_{DM}}{M} \frac{d\sigma(R)}{dM} \frac{\delta_c}{\sigma^2(R, z)} \exp\left(-\frac{\delta_c^2}{2\sigma^2(R, z)}\right), \quad (7)$$

with  $\rho_c$  being the critical density. The factor  $\delta_c$  Eq.(7) is the critical over-density required in a spherical model for gravitational collapse. We take  $\delta_c = 1.28$  following [47]. The other key quantity is  $\sigma^2(R, 0)$ , which is the variance of the density field, obtained using linear perturbation theory, in a sphere of radius  $R$  containing a mean mass  $M$ . Its evolution with respect to redshift is simply given by the growth factor, using the standard factorisation between scale dependence and redshift [49]. The variance of the density field on a scale  $R$  is related to the matter power spectrum  $P(k)$  through convolution with a spherical top-hat window function  $W(kR)$ , with  $R^3 = 3M/4\pi\rho_c\Omega_M$ . To compute the linear matter power spectrum today, we have used CAMB [50]. Both  $P(k)$  and  $\sigma$  are normalized by computing  $\sigma$  in a sphere of  $R = 8h^{-1}\text{Mpc}$ , with  $\sigma_8 = 0.8$  [38, 45].

From the distribution of halo of mass  $M$  at redshift  $z$ , we may compute the flux using

$$\begin{aligned} \mathcal{B}^2(z) &= \bar{\mathcal{B}}^2(z) + B^2(z), \\ &= \rho_c^2 \Omega_{DM}^2 (1+z)^6 \left(1 + \frac{1}{\rho_c^2 \Omega_{DM}^2 (1+z)^3} \int dM \frac{dn}{dM}(z, M) (1+z)^3 \int_0^{r_{vir}(M, z)} dr 4\pi r^2 \rho^2(r, M)\right), \end{aligned} \quad (8)$$

where the first term is the contribution from the smooth distribution of dark matter, which in practice is negligible, and  $\rho(r, M)$  is the dark matter density profile of dark matter in halo. The integral over  $\rho$  is calculated with a cut-off given by the virial radius  $r_{vir}(M, z)$ , which is usually expressed in terms of the so-called concentration parameter  $c_{vir} = r_{vir}(M, z)/r_s$  where  $r_s$  is the core radius which depends on the choice for the profile [51]. The virial radius of a halo of mass  $M$  at a given redshift  $z$  is itself defined as the radius within which the mean density of the halo is  $\Delta_{vir}$  times the smooth density  $\rho_c\Omega_M$ . In the  $\Lambda$ CDM model, this virial over-density is given by

$$\Delta_{vir}(z) = \frac{18\pi^2 + 82(\Omega_M(z) - 1) - 39(\Omega_M(z) - 1)^2}{\Omega_M(z)}. \quad (9)$$

which generalizes the standard result  $\Delta_{vir}(z) = 18\pi^2 \sim 200$  of a CDM universe.

As is standard practice for primordial halos, we consider throughout the paper the Navarro-Frenk-White (NFW) profile as a benchmark [52, 53]. The NFW density profile has a simple analytic expression in terms of the concentration parameter

$$F_{NFW}(c_{vir}) = \frac{c_{vir}^3}{3} \left(1 - \frac{1}{(1 + c_{vir})^3}\right) \left(\text{Log}(1 + c_{vir}) - \frac{c_{vir}}{(1 + c_{vir})}\right)^{-2}. \quad (10)$$

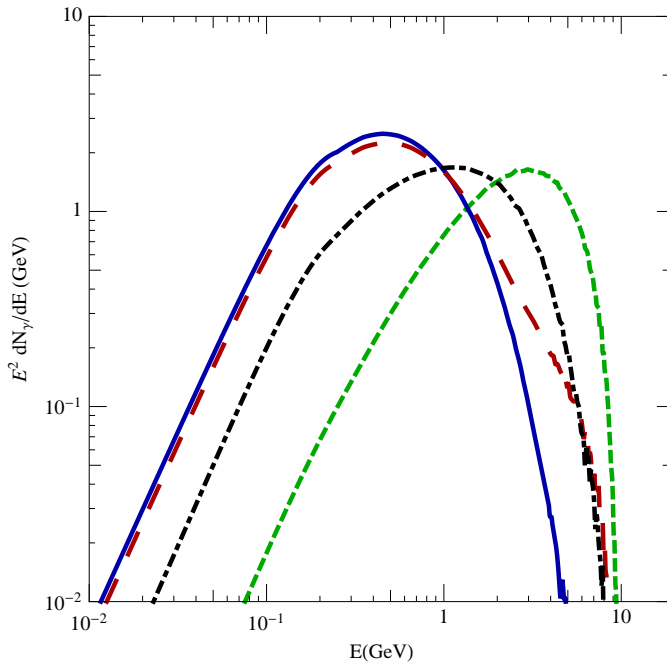


Figure 2: Example of  $E^2 dN_\gamma/dE$  gamma-ray spectra from the annihilation of a 10 GeV dark matter particle, as a function of the photon energy  $E$ . The solid blue line represents a pure annihilation into  $b\bar{b}$  ( $BR_{b\bar{b}} = 100\%$ ), the green dashed curve is for a pure annihilation into  $\tau^+\tau^-$  ( $BR_{\tau^+\tau^-} = 100\%$ ), the red long dashed to a “Higgs-like” annihilation ( $BR_{\tau^+\tau^-} \sim 9\%$  and  $BR_{b\bar{b}} \sim 83\%$ ), while the black dot-dashed line refers to a “Z-like” annihilation ( $BR_{l\pm} \sim 3\%$  and  $BR_{q\bar{q}} \sim 13\%$ ).

Using the previous definitions, the integral over the halo mass function can finally be recast into the form

$$B(z) = \frac{\Delta_{vir}}{3\rho_c\Omega_M} \int_{M_{min}}^{\infty} dM M \frac{dn}{dM} F_{NFW}(c_{vir}(z, M)), \quad (11)$$

where  $M_{min}$  is the minimum halo mass so that Eq. (8) becomes:

$$\mathcal{B}(z) = \rho_c\Omega_{DM}(1+z)^3 \sqrt{1+B(z)}. \quad (12)$$

This is the enhancement factor which appears in the extra-galactic flux, Eq. (1). The dark matter distribution is described by the mean cosmological matter density  $\bar{\mathcal{B}}$  plus the sum over all average enhancements due to a halo of mass  $M$ , weighted over the mass function. The abundance and distribution of halos depend primarily on halo mass and the concentration parameter itself depends on the halo mass at a given redshift. Therefore, the range of  $M_{min}$  and the functional form of  $c_{vir}$  are the major sources of uncertainty in the determination of the diffuse gamma-ray flux and we will discuss our choices in Section III.

### C. Gamma-ray spectrum at production

The last ingredient we will need to compute the contribution to the IGRB, is the spectrum of gamma-rays produced per DM annihilation,

$$\frac{dN_\gamma}{dE} = \sum_f \frac{dN_\gamma^f}{dE} BR_f, \quad (13)$$

where  $dN_\gamma^f/dE$  is the photon spectrum for the  $f$  annihilation final state with branching ratio  $BR_f$ . The gamma-ray spectra from hadronization and final state radiation are calculated with Pythia 8.1 [54]. In Figure 2 we show a few spectra representative of the particle models that we will analyse. The solid blue line is the final state radiation from annihilation into  $b\bar{b}$  pairs, the green short-dashed curve comes from a  $BR = 100\%$  into  $\tau^+\tau^-$ . As is well known, in both cases, the main contribution comes from the decay of neutral pions into gammas, produced from the hadronization

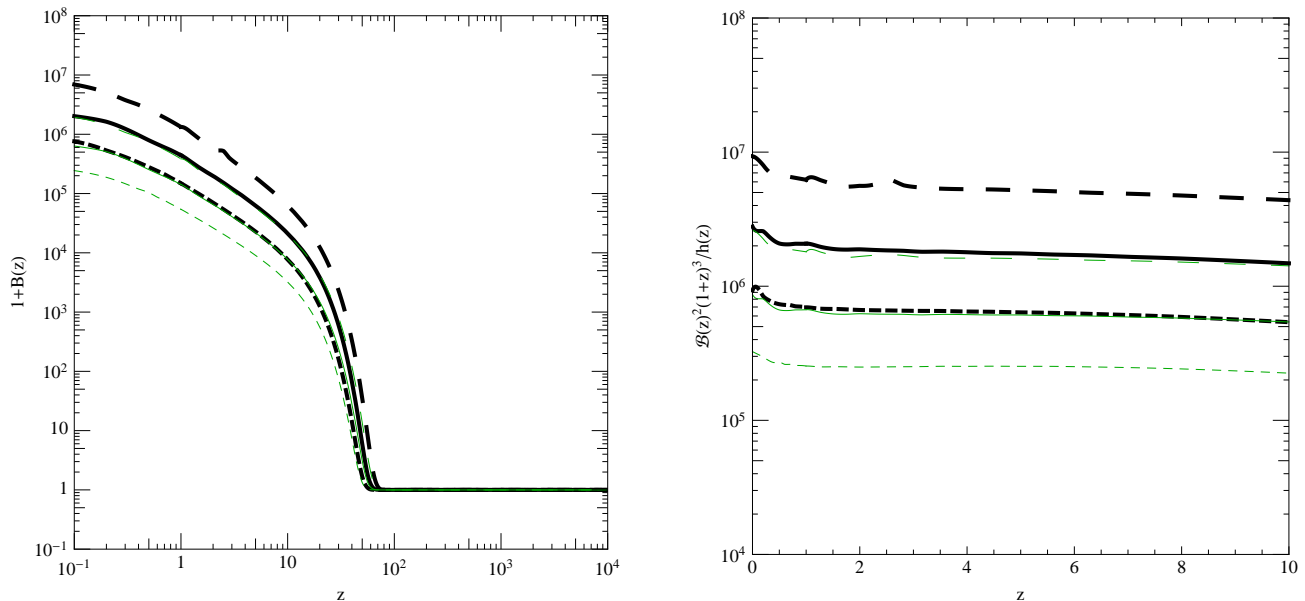


Figure 3: On the left, boost factor  $1 + B(z)$  as a function of the redshift  $z$ . On the right, zoom at small redshift values of the total enhancement factor  $B^2(z)/h(z)(1+z)^3$ . A NFW density profile for the dark matter is assumed. The thin green lines are given for the  $C_{\text{WMAP}}$  concentration parameter [55], while the thick black lines are for the  $C_{\text{PL}}$  concentration parameter [51]. The long dashed lines refer to  $M_{\text{min}} = 10^{-8} M_{\odot}$ , the solid to  $M_{\text{min}} = 10^{-6} M_{\odot}$  and the short dashed to  $M_{\text{min}} = 10^{-4} M_{\odot}$ .

of the  $b\bar{b}$  pair or from the semi-hadronic decay of the  $\tau^+\tau^-$ . The most relevant feature for our analysis, which will make use of the lower energy edge of the Fermi-LAT data, is that the photon spectrum from  $\tau^+\tau^-$  is harder than the one from  $b\bar{b}$  quarks. The red long-dashed curve is the photon spectrum for light WIMP with ‘‘Higgs-like’’ coupling to SM degrees of freedom, namely with a branching ratio dictated by the Yukawa couplings. For instance, for a scalar dark matter particle with  $M_{DM} = 10$  GeV, it corresponds to a  $BR_{b\bar{b}} = 83\%$  and to a  $BR_{\tau^+\tau^-} = 9\%$ . The black dot-dashed line is the spectrum for a DM particle with ‘‘Z-like’’ couplings, in which case  $BR_{b\bar{b}} \sim 3 \times BR_{l\pm} \sim 13\%$ .

### III. GENERAL RESULTS REGARDING A LIGHT WIMP

In this section we discuss, and compare to known results, our choice for astrophysical quantities like the concentration parameters and the minimum DM halo mass that may form. These parameters are defined in a non-unique way in the literature, and the choice of their parametrization will affect the limits on the annihilation cross-sections. Once the technical details are worked out, we present some generic constraints relevant for a light WIMP, with  $M_{DM}$  up to 20 GeV.

#### A. Uncertainties from structure formation

Simulation of halos [51, 52] indicate that there is a strong correlation between the concentration parameter and the halo mass  $M$ . Among other properties, they are inversely related, *e.g.* higher mass halos are less concentrated. A model that fits the results of the simulations is:

$$c_{vir}(z, M) = \frac{c_{vir}(0, M)}{1+z}, \quad (14)$$

meaning that  $c_{vir}$  is inversely proportional to the redshift as the radius of a halo increases as the universe expands. We use two different power law fits for  $c_{vir}$ : the WMAP-5yrs best fit in [55] ( $C_{\text{WMAP}}$  hereafter) and a simple power-law behavior,  $c_{vir} \propto M^{-0.1}$ , as indicated by numerical simulations [51] ( $C_{\text{PL}}$  from now on).

The other quantity that affects the final results, namely the upper bounds on  $\langle \sigma v \rangle_{ann}$ , is the choice of the minimal halo mass, appearing as the lower limit in the integral of Eq. (11). It has been shown in [56, 57] that free streaming and collisional damping of a WIMP with the radiation component lead to a small-scale cut-off in the DM density

perturbation power spectrum. The size of the smallest gravitationally bound structure is set by the properties of the WIMP. After the DM particle abundance has frozen out in the early universe, it may stay in local thermal equilibrium by elastic scattering processes with relativistic particles  $DM + f \rightarrow DM + f$ . As the universe expands the WIMP density decreases, the elastic scattering rate decreases and the WIMPs kinetically decouples at a temperature  $T_{\text{kd}}$ . From this moment on the WIMPs can stream freely and wash out any matter contrast on small scales. The complete decoupling from the thermal bath usually happens when the temperature has dropped by a factor  $\sim 10 - 1000$  with respect to the chemical decoupling temperature, namely  $T_{\text{kd}} \sim \mathcal{O}(\text{MeV})$ . This is indeed true for models where the DM particle interacts with leptons, especially electrons, that are a relativistic species at that time. In the next section we will consider two distinct light WIMP candidate, one with “Z-like” couplings to SM degrees of freedom, and for which kinetic coupling occurs at a MeV scale, as can be estimated from [58]. We will also consider a candidate with “Higgs-like” couplings to ordinary matter, *i.e.* through Yukawa couplings. In that case kinetic decoupling occurs at about the same time as the chemical decoupling, typically  $T_{\text{kd}} \sim \text{few hundreds MeV}$ . Once the kinetic decoupling temperature is known, we estimate the free streaming length  $k_{\text{fs}}$  from [59]. The mass of the smallest bound structure is given by  $M_{\text{fs}} = 4/3 \rho_{\text{DM}} (\pi/k_{\text{fs}})^3 M_{\odot}$ . For the case of the “Z-like” candidate we obtain  $M_{\text{min}} \sim 10^{-5} M_{\odot}$ , while for “Higgs-like” couplings we get  $M_{\text{min}} \sim 10^{-7} M_{\odot}$ . We also consider the results of Ref. [60], which are based on a numerical evaluation of  $k_{\text{fs}}$ ; in this case using the same kinetic decoupling temperature as before, we obtain limits that are one order of magnitude lower,  $M_{\text{min}} = 10^{-8} M_{\odot}$  ( $M_{\text{min}} = 10^{-6} M_{\odot}$ ) for “Higgs-like” (resp. “Z-like”) couplings. Consequently, in the evaluation of the diffuse gamma-ray signals we consider three different minimum mass values:  $M_{\text{min}} = 10^{-8}, 10^{-6} M_{\odot}$  and  $10^{-4} M_{\odot}$  for the model independent and for the singlet case, while only two values for the “Z-like” DM candidate,  $M_{\text{min}} = 10^{-6} M_{\odot}$  and  $10^{-4} M_{\odot}$ . For these models the minimum mass allowed by acoustic oscillations is far below the smallest halo mass permitted by the free streaming length scale  $k_{\text{fs}}$  [59].

We show in Figure 3 the boost, Eq. (11), and total enhancement factor, Eq. (12), as a function of the redshift  $z$ . The green thin lines are for the  $C_{\text{WMAP}}$  concentration parameter, while the black thick curves match the simple power law behavior for  $c_{\text{vir}}$ . The long-dashed lines correspond to  $M_{\text{min}} = 10^{-8} M_{\odot}$ , the solid curves to  $M_{\text{min}} = 10^{-6} M_{\odot}$  and finally the short-dashed to  $M_{\text{min}} = 10^{-4} M_{\odot}$  (the same convention for the curves description is maintained throughout the paper). On the left panel, we see that the enhancement due to structure formation starts to dominate over the smooth component at  $z \leq 30$ . The boost depends crucially on the concentration parameter, as  $C_{\text{WMAP}}$  leads to smaller boosts with respect to  $C_{\text{PL}}$ ; this has already been shown in [61], and we found agreement with their results. In the case of the  $C_{\text{WMAP}}$  parameterization we have checked that our results are equivalent to those in Fig. (1) of Ref. [37]. On the right-hand side we show a zoom of the total dark matter density at small redshifts, the same quantity represented in Fig.(1) of Ref. [36]. The Fermi-LAT collaboration has used a different approach to compute the dark matter halo distribution, however we may compare their analytical estimation (labeled *BulSub*) with our calculations with  $M_{\text{min}} = 10^{-6} M_{\odot}$ : for  $C_{\text{WMAP}}$  we are 10% below their estimation, while for  $C_{\text{PL}}$  our boost is a factor  $\sim 3$  above their curve. It is this small difference in the boost value at small redshifts (which are the values that contribute the most to the diffuse photon flux for a light WIMP) that will explain our more stringent upperbounds. We note that for a given concentration parameter and  $M_{\text{min}} = 10^{-6} M_{\odot}$ , the value  $M_{\text{min}} = 10^{-8}(10^{-4}) M_{\odot}$  corresponds to increase (decrease) the boost by a factor  $\sim 3$ . Even though the diffuse photon flux is also increased or decreased by the same amount, below we show the upper bounds for all the  $M_{\text{min}}$  cases and for the two fit of the  $c_{\text{vir}}$ .

Finally, one should keep in mind the uncertainty related in the choice of profile, here a NFW. Less cuspy profiles, like Einasto [62] or Burkert [63], will give a smaller boost, typically by a factor of 3 in the former case, and a factor of 8 in the latter [37].

## B. Discussion on the upper bounds

The measured fluxes  $\phi_i^{\text{IGRB}}$  and the errors  $\sigma_i$  for the diffuse emission are those given by the Fermi-LAT collaboration, listed in Table I of [32] in the energy range from 0.2 GeV up to 102.4 GeV. The measurements arise from a full sky fit, for latitude  $\geq 10^\circ$  and from the data of the initial 10 months of the Fermi mission. From the isotropic diffuse component measured by Fermi, the IGRB flux is obtained subtracting the diffuse galactic emission, point sources and a cosmic rays background. The measured IGRB spectrum is compatible with a featureless power law with index  $-2.41$  [32]. In this light we derive conservative upper bounds on the annihilation cross-section of a WIMP, namely the dark matter signal should not exceed the measured flux in any individual bin  $i$  by more than a given amount

$$\phi_i^{\text{th}} \leq \phi_i^{\text{IGRB}} + n \sigma_i. \quad (15)$$

The index  $n$  indicates the significance of the upper bound,  $n = 1.64$  corresponds to the 95% confidence level (C.L.), assuming that the probability distributions for the intensity in each bin are Gaussian and independent from each other. The limits on the DM annihilation rate are derived taking the lowest value of  $\langle \sigma v \rangle_{\text{ann}}$  for which Eq. (15) is

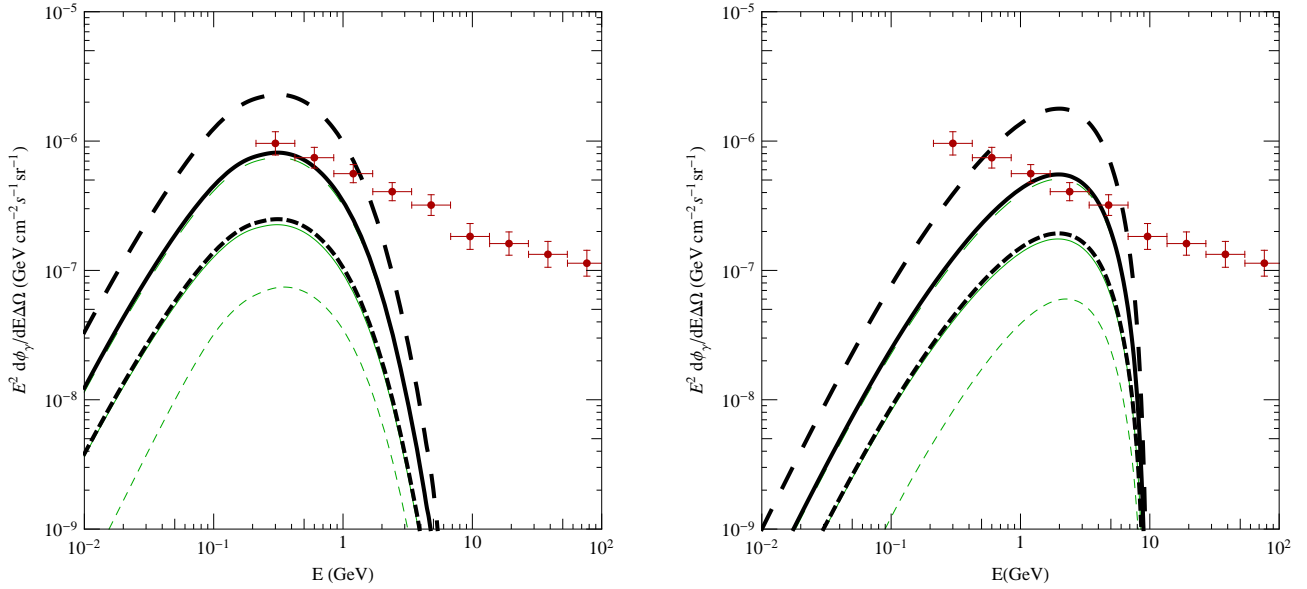


Figure 4: Diffuse photon emission from a 10 GeV dark matter particle for  $BR_{b\bar{b}} = 100\%$  on the left, and with annihilation into  $BR_{\tau^+\tau^-} = 100\%$  on the right. For the  $b\bar{b}$  channel  $\langle\sigma v\rangle_{ann} = 2.6 \cdot 10^{-26} \text{ cm}^3 \text{ s}^{-1}$ , while for the  $\tau^+\tau^-$  case the thermal cross-section is fixed to  $3.3 \cdot 10^{-26} \text{ cm}^3 \text{ s}^{-1}$ . The color code is as in Fig. 3. The red points are the measurements of the diffuse emission by Fermi-LAT [32].

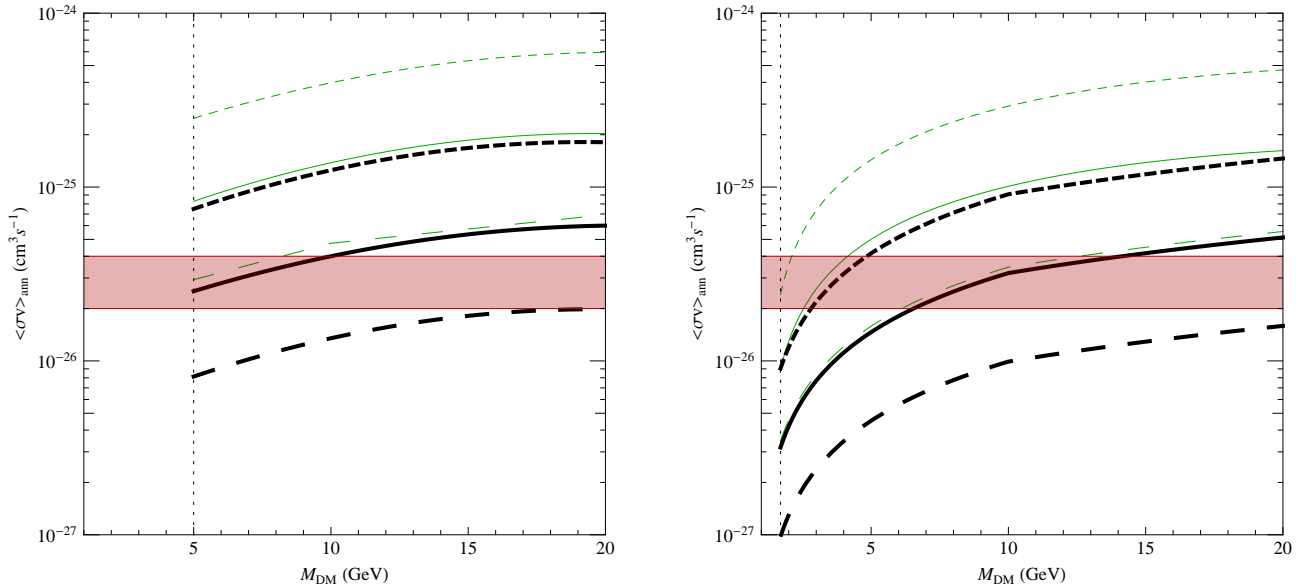


Figure 5: Upper bounds in the plane  $\langle\sigma v\rangle_{ann}$  versus the DM mass  $M_{DM}$  at 95% C.L. for two different annihilation channels: on the left  $BR_{b\bar{b}} = 100\%$  and on the right  $BR_{\tau^+\tau^-} = 100\%$ . The horizontal red (gray) region indicates the typically preferred value for the thermal annihilation cross-section. The color code is as in Fig. 3.

not satisfied. In order to explain the Fermi IGRB data one needs to add a background contribution in each energy bin where the DM flux is too small to account for the measured intensity.

In Figure 4, the predicted IGRB photon flux times  $E^2$  as a function of the photon energy is shown for a 10 GeV DM particle that annihilates with a branching ratio of 100% into  $b\bar{b}$  or  $\tau^+\tau^-$  together with the Fermi-LAT data (red bins). For the  $b\bar{b}$  model, a  $\langle\sigma v\rangle_{ann} = 2.6 \cdot 10^{-26} \text{ cm}^3 \text{ s}^{-1}$  is already excluded for  $M_{min} = 10^{-8} M_\odot$  and  $c_{vir} = C_{PL}$ , while it is fully compatible for  $M_{min} = 10^{-6} M_\odot$  and  $c_{vir} = C_{PL}$  or  $M_{min} = 10^{-8} M_\odot$  and  $c_{vir} = C_{WMAP}$ . From the shape of the flux, we see that the upper bounds will come from the first, second or at most third bin (depending on the dark matter mass) of the Fermi-LAT data, namely from measured photon energies lower than 2 GeV. The  $\tau^+\tau^-$



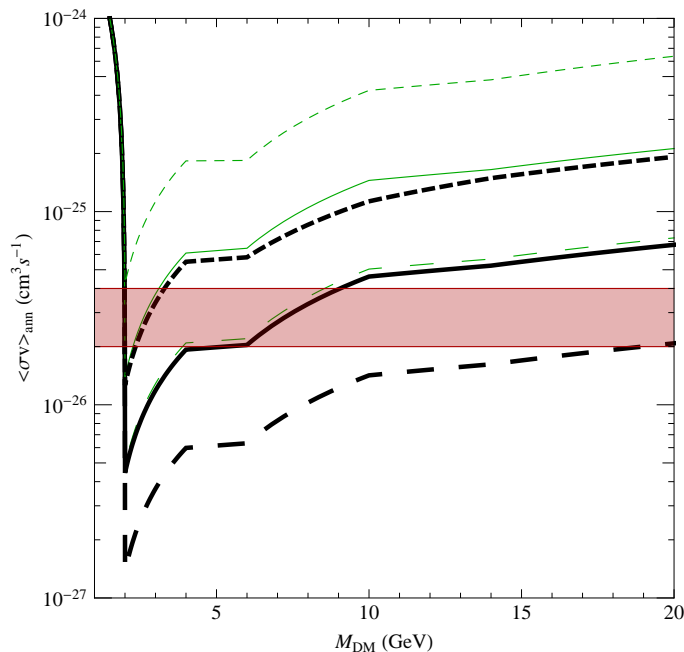


Figure 6: The same as in Fig. 5 for the singlet dark matter candidate with “Higgs-like” annihilation channels.

case is analogous, again  $M_{\min} = 10^{-8} M_{\odot}$  and  $c_{\text{vir}} = C_{\text{PL}}$  excludes a cross-section of  $3.3 \cdot 10^{-26} \text{cm}^3 \text{s}^{-1}$ , while this value is perfectly compatible for all other configurations of the astrophysical parameters. However in this case the most constraining energy bins are from the second to the fifth: the relevant energy range is more close to the photon production threshold, namely the dark matter mass. The contribution to the extra galactic photon flux comes from low redshifts.

Scanning over the mass range from 1 GeV up to 20 GeV, we obtain the upper bounds in the plane  $\langle \sigma v \rangle_{\text{ann}}$  vs the dark matter mass  $M_{\text{DM}}$ , Figure 5. The pure  $b\bar{b}$  final state case is the left panel, while the right plot is given for an annihilation into  $\tau^+\tau^-$ . Comparing these two model-independent cases, we note that the leptonic final state give more stringent upper bounds, for the same assumption on the astrophysical parameters, due to the different shape of the photon spectrum. In example, the  $\langle \sigma v \rangle_{\text{ann}}$  values that lead to a relic abundance in the WMAP range, are always compatible with the Fermi data for  $BR_{b\bar{b}} = 100\%$ , while they are excluded at 95% C.L. for  $BR_{\tau^+\tau^-} = 100\%$  and  $M_{\text{DM}} \leq 7$  GeV, with  $M_{\min} = 10^{-6} M_{\odot}$  and  $C_{\text{PL}}$ . As already noted, the different choice in  $M_{\min}$  moves up or down the bounds by a factor of  $\sim 3$ . The bounds from the  $b\bar{b}$  are compatible with those in [34, 36]. The pure  $\tau^+\tau^-$  has not yet been discussed for such low DM masses.

#### IV. SOME MODEL-DEPENDENT RESULTS

One may say that they are essentially two classes of models of dark matter. To the first class belong models within which dark matter is a by-product, the secondary effect of a deeper goal. Such are the neutralino and the axion, and, to some extent, DM candidates in theories with extra dimensions (for a review see [64]). The other class encompasses the many models which start with the DM problem, sometime in a minimalistic way, sometime with a broader scope in mind. The first class may be nobler, but, with the advent of new data, the bottom-up approach to DM has gained some momentum. In particular, the interpretation of the CoGeNT or DAMA data as being due to DM has motivated much works, both on the possibility to explain the data with a light neutralino [65–71] and on new models (see *e.g.* [5, 6, 30, 67–69, 72–83]). In this section, for the sake of illustration, we consider two simple light WIMP candidates. These models have in common the facts that they are based on minimal extensions of the SM and yet may explain the direct detection data while having a relic abundance that agrees with cosmological observations. The first model is based on a real scalar singlet, which is interacting through the Higgs portal with the SM degrees of freedom [31, 84, 85]. The second model invokes a singlet Dirac fermion, interacting through the kinetic mixing portal, *i.e.* via a new  $Z'$  gauge boson [83, 86, 87].

That a real scalar singlet interacting through the Higgs may be in agreement with both CoGeNT-DAMA and WMAP has been argued in [9, 31, 88]. This is implicit in other works. In particular in the results of [8], which

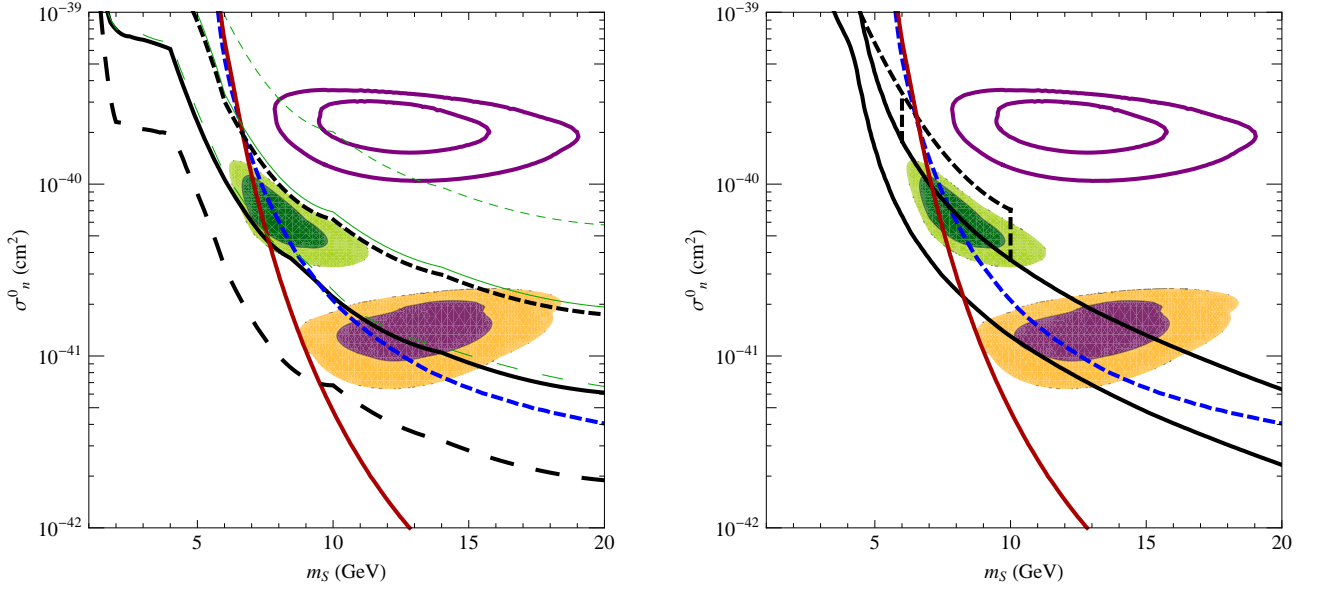


Figure 7: On the left, SI cross-section ( $\sigma_n^0$ ) vs scalar singlet mass ( $m_S$ ). The green region corresponds to CoGeNT [3] (minimum  $\chi^2$ , with contours at 90 and 99.9% C.L.). The DAMA regions [2] (goodness-of-fit, also at 90 and 99.9% C.L.) are given both with (purple/orange) and without (purple, no fill) channelling. The blue (short-dashed) line is the 90% C.L. exclusion limit from CDMS-Si [15]. The red solid curve is the 90% exclusion limit from Xenon100 [19], using LeffMin and a threshold at 3 PhotoElectron. For more details on the experimental upper bounds and conventions see [9]. The black thick and green thin lines are as in Fig. 3 and denote the exclusion limits from the Fermi-LAT diffuse gamma-rays flux at 95% C.L.. On the right, same as the left panel but instead of the exclusion limit from the Fermi-LAT measurements we include the region the  $\sigma_n^0 - m_S$  consistent with WMAP. The continuous region corresponds to the standard assumption of a QCD phase transition at  $T_c = 150$  MeV. The black dashed lines correspond, from left to right, to the border of the WMAP region for  $T_c = 300$  MeV and  $T_c = 500$  MeV respectively.

are based on an effective operator approach (see in particular Figure 4, lower left plot). We may also refer to [81], which is based on a singlet complex scalar, in particular Figure 7. In practice, these models differ only in the choice of couplings to the SM degrees of freedom, which in the case of [9, 31] are simply proportional to the SM fermions mass (“Higgs-like” couplings) and thus more constrained. These scalar DM models also have in common the fact that, at the low energies relevant for the CoGeNT-DAMA regions and the calculation of the relic abundance from freeze-out, the ratio of the annihilation and elastic scattering on nuclei cross-sections only depends on the DM mass. In particular, for the case of one real scalar singlet  $S$  of mass  $m_S$  interacting through the Higgs, the ratio is

$$\sum_f \frac{\sigma(SS \rightarrow \bar{f}f)v_{rel}}{\sigma(SN \rightarrow SN)} = \sum_f \frac{n_c m_f^2}{f^2 m_N^2 \mu_n^2} \frac{(m_S^2 - m_f^2)^{3/2}}{m_S}, \quad (16)$$

where  $n_c = 3(1)$  for quarks (leptons),  $\mu_n$  is the DM-nucleon reduced mass and the factor  $f$  parametrizes the Higgs to nucleons coupling from the trace anomaly, which has central value  $f \sim 0.3$  [31]. Taking into account the branching ratio for annihilation of a light  $S$  into SM fermions (essentially 100%  $b\bar{b}$  for  $m_S \sim 10$  GeV, up to 10% in  $\tau^+\tau^-$  for  $m_S \sim 6$  GeV and  $\mathcal{O}(50\%)$  in  $\tau^+\tau^-$  below  $\sim 5$  GeV), the limits on the annihilation cross-section of the  $S$  from the IGRB measured by Fermi-LAT are shown in Figure 6. Which limiting curve we may believe is most relevant depends strongly on the minimum halo mass  $M_{min}$ . An interesting feature is that, after freeze-out, a particle with “Higgs-like” couplings to SM degrees of freedom, has very little interactions with particles from the plasma. Indeed we may neglect the Yukawa coupling with the electron and positrons, while the protons and neutrons are very few in the plasma. Using Eq.(13) of Ref.[59], we then estimate  $M_{min} \sim 10^{-8} M_\odot$  taking the kinetic coupling temperature to be of the order of the chemical decoupling temperature. To this parameter, together with  $C_{PL}$ , corresponds the strongest constraint we may get based on the IGRB (long dashed curves in Figure 6). In this plot we see that all the  $\langle \sigma v \rangle_{ann}$  values that account for the WMAP abundance are excluded at 95% C.L., while more relaxed constraints come from either  $M_{min} = 10^{-6} M_\odot$  and  $C_{PL}$  (solid black thick curve) or  $M_{min} = 10^{-8} M_\odot$  and  $C_{WMAP}$  (solid thin green line). Annihilation cross-sections of the order  $3 \cdot 10^{-26} \text{cm}^3 \text{s}^{-1}$  are excluded only for very light scalar masses,  $m_S \leq 7$  GeV.

Furthermore, using the Eq.(16), we may transpose the limits on the annihilation cross-section into limits on the

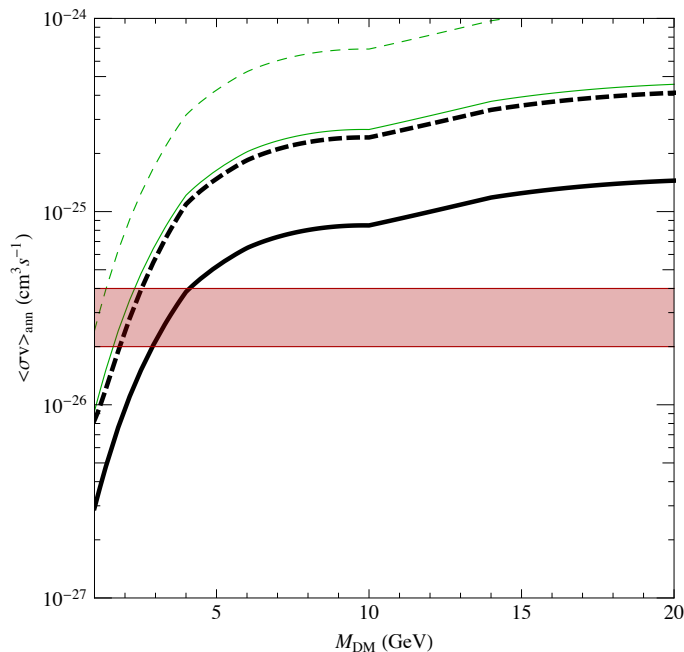


Figure 8: The same as in Fig. 6 for the singlet Dirac fermion candidate, through annihilation channels with “Z-like” couplings.

elastic scattering cross-section on nuclei, and plot them in the  $\sigma_n^0 - m_S$  plane, Figure 7 on the left, together with the CoGeNT-DAMA regions and the exclusion limits set by CDMS-Si and Xenon100, which were computed as in [9]. Following the same convention as in the other figures, the upper bounds from the IGRB are shown in green or black. For  $M_{\min} = 10^{-8} M_\odot$  and a power law concentration parameter the DAMA and CoGeNT regions are both excluded at 95% C.L., while the same minimum halo mass with  $C_{\text{WMAP}}$  gives limits which are marginally compatible with the CoGeNT region. A choice of  $M_{\min} = 10^{-6} M_\odot$  and  $C_{\text{WMAP}}$  is totally compatible with the CoGeNT region and can be accommodated with the DAMA region (see footnote 4).

For comparison, we also give in Figure 7 (right panel) the region of the  $\sigma_n^0 - m_S$  plane consistent with WMAP. In this latest figure, the black continuous line is based on the hypothesis that the QCD phase transition occurred at a temperature  $T_c = 150$  MeV (which is the standard assumption both for DarkSusy [89] and Micromegas [90]). Freeze-out after the QCD phase transition would require an annihilation cross-section which is about twice that for a standard WIMP,  $\langle \sigma v \rangle_{\text{ann}} \sim 3 \cdot 10^{-26} \text{ cm}^3 \text{ s}^{-1}$  (see for instance [65]). Since typically  $x_f = M_{\text{DM}}/T_f \sim 20$ , this effect is only relevant for  $M_{\text{DM}} \lesssim 3$  GeV. However, we may contemplate the possibility that the QCD phase transition took place at a higher temperature, for instance  $150 \text{ MeV} < T_c < 500 \text{ MeV}$ , which is relevant for a candidate  $M_{\text{DM}} \lesssim 10$  GeV, and thus for the CoGeNT-DAMA regions<sup>4</sup>.

For the sake of comparison, we consider a model that consists of a singlet Dirac fermion candidate  $\psi$ , charged under a broken  $U(1)'$  gauge group, which may interact with the SM degrees of freedom through the kinetic mixing portal. In [83], it has been shown that such a candidate may be consistent with both WMAP and the CoGeNT-DAMA regions as well as constraints from LEP1 on the  $Z$  invisible width. We notice that this result is *a priori* in contradiction with the one drawn in [31] and [8], where it has been shown that a singlet Dirac DM candidate (for a single, vector or scalar annihilation channel) that fits the CoGeNT-DAMA regions has a too large relic abundance. However, there is no magic, as the conclusion in [8, 31] has been reached by assuming that there exist a one-to-one correspondence between the annihilation and scattering cross-section (for fixed dark matter mass), while in [83] the proximity of the  $Z'$  pole is used to enhance this annihilation cross-section so as to get the right relic abundance. Incidentally, this will prevent us from presenting the exclusion limits in the  $\sigma_n^0 - M_{\text{DM}}$  plane for this model, for the ratio of  $\langle \sigma v \rangle_{\text{ann}}$

<sup>4</sup> This effect may be relevant in the light of the many possible uncertainties that may be hidden in a Figure like 7 (plot on the right). For instance, in [23], it is argued that channelling may, after all, not be very relevant for the interpretation of the DAMA data, so the lower of the two regions corresponding to DAMA most presumably does not exist. There is however still substantial freedom just on the experimental side, and, based on the current uncertainties on parameters like quenching, the authors of [14] argued quite convincingly that, not only, both the DAMA (without channelling) and CoGeNT may be consistent with each other but, moreover, are not excluded by the current exclusion limits.

and  $\sigma_n^0$  depends on  $M_{Z'}$  and  $\Gamma_{Z'}$ ,

$$\sum_f \frac{\sigma(\bar{\psi}\psi \rightarrow \bar{f}f)v_{rel}}{\sigma(\psi N \rightarrow \psi N)} = \sum_f \frac{n_c}{4} \frac{\left(1 - \frac{m_f^2}{m_\psi^2}\right)^{1/2}}{\mu_n^2} \left( \left(1 - \frac{4m_\psi^2}{M_{Z'}^2}\right)^2 + \frac{\Gamma_{Z'}^2}{M_{Z'}^2} \right)^{-1} \left( 2m_\psi^2(v_f^2 + a_f^2) + (v_f^2 - a_f^2)m_f^2 \right). \quad (17)$$

In Eq.(17),  $a_f$  and  $v_f$  are the SM model axial and vector couplings of the fermions to the  $Z$ . The limits on the annihilation cross-section of  $\psi$  from the IGRB are shown in Figure 8. That the  $Z'$  has “Z-like” couplings to the SM degrees of freedom (compared to the “Higgs-like” couplings of the scalar singlet) has two interesting consequences regarding the constraints from the IGRB. First the annihilation channels are distinct, with a spectrum that is harder with respect to the scalar singlet one, and lead to the constraints from Fermi-LAT to extend to rather light DM candidates. Also, because of the abundance of the  $e^+e^-$  pairs (and neutrinos) in the thermal bath, the kinetic decoupling (compared to the chemical freeze-out that fixes the relic abundance) of a DM candidate with “Z-like” couplings occurs at a much smaller temperature, which, following [59], we estimate to be  $\mathcal{O}(1 \text{ MeV})$ . This implies that the minimum halo mass that may form in the model is substantially larger for the Dirac fermion than in the case of the singlet scalar,  $M_{min} \sim 10^{-4}M_\odot$ . This is the reason why we only plot the the exclusion limits for  $M_{min} \sim 10^{-6}M_\odot$  (which is very optimistic) and  $M_{min} \sim 10^{-4}M_\odot$  (which is presumably more realistic) in Figure 8. In this case the most stringent limit, given by  $M_{min} = 10^{-6}M_\odot$  and  $C_{PL}$  excludes at 95% C.L. the WMAP region for  $m_\psi < 5 \text{ GeV}$ . All the other curves only marginally affect  $\langle \sigma v \rangle_{ann} \sim 3 \cdot 10^{-26} \text{ cm}^3 \text{ s}^{-1}$ .

Altogether, we may conclude that, although they are both viable candidates with respect to WMAP and CoGeNT-DAMA, the constraints from the IGRB are substantially weaker for the  $\psi$  candidate, with “Z-like” couplings, than for the  $S$  candidate with “Higgs-like” couplings.

## V. CONCLUSIONS

In this work, we have studied the constraints that may be set, using the Fermi-LAT data on the isotropic diffuse gamma-ray emission, on the parameter space of two simple, albeit generic, DM candidates, which has been shown to be consistent both with the WMAP relic abundance, and the regions favoured by CoGeNT-DAMA [9, 83]. The constraints we get are consistent with results which may be inferred from other current works on constraints on DM from extragalactic gamma-ray fluxes [34, 36]. We have however extended them to lower DM masses and make explicitly the connection with the CoGeNT-DAMA results tentatively interpreted as being due to the elastic scattering of DM particles. Our main results are summarized in Figure 6 for the case of a singlet scalar candidate  $S$  interacting through the Higgs portal (“Higgs-like” couplings to SM degrees of freedom) and Figure 8 for the case of Dirac fermion candidate  $\psi$  interacting through a  $Z'$  (“Z-like” couplings). In the former case, we have used the one-to-one correspondence between the elastic cross-section and the annihilation cross-section, Eq.(16) to express the limit from the isotropic gamma-ray background radiation (IGRB) directly in the  $\sigma_n^0 - m_S$  plane, Figure 7. In particular, this shows that the CoGeNT-DAMA regions may be constrained using the recent Fermi-LAT data, at least for the case of the scalar dark matter candidate. Needless to say, such constraints should be taken with a grain of salt, as they suffer from the usual astrophysical uncertainties, regarding for instance the profile of dark matter in halos, and other parameters which enter in the estimation of the extragalactic boost (even the use of the Press-Schechter formula may be a matter of discussion, as is the extrapolation of over many decades of the known power spectrum of the DM inhomogeneities). Regarding the profile we have chosen use the somewhat standard NFW choice, like in [35, 36]; clearly a different choice, like the Einasto or Burkert profiles would give less stringent constraints.

## Acknowledgments

One of us (M.T.) would like to thank Y. Mambrini for useful discussions. Our work is supported by the FNRS-FRS, the IISN and the Belgian Science Policy (IAP VI-11).

- 
- [1] E. Komatsu *et al.*, (2010), arXiv:1001.4538.
  - [2] DAMA, R. Bernabei *et al.*, Eur. Phys. J. **C56**, 333 (2008), arXiv:0804.2741.
  - [3] CoGeNT, C. E. Aalseth *et al.*, (2010), arXiv:1002.4703.
  - [4] W. S. at *WONDER2010* and J. C. at *Light Dark Matter* workshop at UC Davis, (2010).

- [5] F. Petriello and K. M. Zurek, JHEP **09**, 047 (2008), arXiv:0806.3989.
- [6] C. Savage, G. Gelmini, P. Gondolo, and K. Freese, (2008), arXiv:0808.3607.
- [7] J. Kopp, T. Schwetz, and J. Zupan, (2009), arXiv:0912.4264.
- [8] A. L. Fitzpatrick, D. Hooper, and K. M. Zurek, (2010), arXiv:1003.0014.
- [9] S. Andreas, C. Arina, T. Hambye, F.-S. Ling, and M. H. G. Tytgat, (2010), arXiv:1003.2595.
- [10] S. Chang, J. Liu, A. Pierce, N. Weiner, and I. Yavin, (2010), arXiv:1004.0697.
- [11] V. A. Kudryavtsev, M. Robinson, and N. J. C. Spooner, (2009), arXiv:0912.2983.
- [12] J. P. Ralston, (2010), arXiv:1006.5255.
- [13] R. Bernabei *et al.*, (2010), arXiv:1007.0595.
- [14] D. Hooper, J. I. Collar, J. Hall, and D. McKinsey, (2010), arXiv:1007.1005.
- [15] CDMS, D. S. Akerib *et al.*, Phys. Rev. Lett. **96**, 011302 (2006), arXiv:astro-ph/0509259.
- [16] The CDMS-II, Z. Ahmed *et al.*, (2009), arXiv:0912.3592.
- [17] J. Angle *et al.*, Phys. Rev. Lett. **101**, 091301 (2008), arXiv:0805.2939.
- [18] XENON10, J. Angle *et al.*, Phys. Rev. **D80**, 115005 (2009), arXiv:0910.3698.
- [19] XENON100, E. Aprile *et al.*, (2010), arXiv:1005.0380.
- [20] J. I. Collar and D. N. McKinsey, (2010), arXiv:1005.0838.
- [21] T. X. Collaboration, (2010), arXiv:1005.2615.
- [22] J. I. Collar and D. N. McKinsey, (2010), arXiv:1005.3723.
- [23] C. Savage, G. Gelmini, P. Gondolo, and K. Freese, (2010), arXiv:1006.0972.
- [24] J. I. Collar, (2010), arXiv:1006.2031.
- [25] J. L. Feng, J. Kumar, J. Learned, and L. E. Strigari, JCAP **0901**, 032 (2009), arXiv:0808.4151.
- [26] S. Andreas, M. H. G. Tytgat, and Q. Swillens, JCAP **0904**, 004 (2009), arXiv:0901.1750.
- [27] V. Niro, A. Bottino, N. Fornengo, and S. Scopel, Phys. Rev. **D80**, 095019 (2009), arXiv:0909.2348.
- [28] J. Goodman *et al.*, (2010), arXiv:1005.1286.
- [29] Y. Bai, P. J. Fox, and R. Harnik, (2010), arXiv:1005.3797.
- [30] J. L. Feng, J. Kumar, and L. E. Strigari, Phys. Lett. **B670**, 37 (2008), arXiv:0806.3746.
- [31] S. Andreas, T. Hambye, and M. H. G. Tytgat, JCAP **0810**, 034 (2008), arXiv:0808.0255.
- [32] The Fermi-LAT, A. A. Abdo *et al.*, Phys. Rev. Lett. **104**, 101101 (2010), arXiv:1002.3603.
- [33] M. Papucci and A. Strumia, JCAP **1003**, 014 (2010), arXiv:0912.0742.
- [34] K. N. Abazajian, P. Agrawal, Z. Chacko, and C. Kilic, (2010), arXiv:1002.3820.
- [35] G. Hutsi, A. Hektor, and M. Raidal, (2010), arXiv:1004.2036.
- [36] Fermi-LAT, A. A. Abdo *et al.*, JCAP **1004**, 014 (2010), arXiv:1002.4415.
- [37] M. Cirelli, F. Iocco, and P. Panci, JCAP **0910**, 009 (2009), arXiv:0907.0719.
- [38] P. Ullio, L. Bergstrom, J. Edsjo, and C. G. Lacey, Phys. Rev. **D66**, 123502 (2002), arXiv:astro-ph/0207125.
- [39] T. R. Slatyer, N. Padmanabhan, and D. P. Finkbeiner, Phys. Rev. **D80**, 043526 (2009), arXiv:0906.1197.
- [40] G. R. Blumenthal and R. J. Gould, Rev. Mod. Phys. **42**, 237 (1970).
- [41] F. A. Agaronyan, A. M. Atoyan, and A. M. Nagapetyan, Astrophysics **19**, 187 (1983).
- [42] A. A. Zdziarski and R. Svensson, Nucl. Phys. Proc. Suppl. **10B**, 81 (1989).
- [43] R. C. Gilmore, P. Madau, J. R. Primack, R. S. Somerville, and F. Haardt, (2009), arXiv:0905.1144.
- [44] F. W. Stecker, M. A. Malkan, and S. T. Scully, Astrophys. J. **648**, 774 (2006), arXiv:astro-ph/0510449.
- [45] A. Natarajan and D. J. Schwarz, Phys. Rev. **D78**, 103524 (2008), arXiv:0805.3945.
- [46] A. Cooray and R. K. Sheth, Phys. Rept. **372**, 1 (2002), arXiv:astro-ph/0206508.
- [47] R. Barkana and A. Loeb, Astrophys. J. **609**, 474 (2004), arXiv:astro-ph/0310338.
- [48] W. H. Press and P. Schechter, Astrophys. J. **187**, 425 (1974).
- [49] D. J. Eisenstein and W. Hu, Astrophys. J. **511**, 5 (1997), arXiv:astro-ph/9710252.
- [50] A. Lewis, A. Challinor, and A. Lasenby, Astrophys. J. **538**, 473 (2000), arXiv:astro-ph/9911177.
- [51] J. S. Bullock *et al.*, Mon. Not. Roy. Astron. Soc. **321**, 559 (2001), arXiv:astro-ph/9908159.
- [52] J. F. Navarro, C. S. Frenk, and S. D. M. White, Astrophys. J. **490**, 493 (1997), arXiv:astro-ph/9611107.
- [53] J. F. Navarro *et al.*, (2008), arXiv:0810.1522.
- [54] T. Sjostrand, S. Mrenna, and P. Z. Skands, Comput. Phys. Commun. **178**, 852 (2008), arXiv:0710.3820.
- [55] A. V. Maccio', A. A. Dutton, and F. C. v. d. Bosch, (2008), arXiv:0805.1926.
- [56] S. Hofmann, D. J. Schwarz, and H. Stoecker, Phys. Rev. **D64**, 083507 (2001), arXiv:astro-ph/0104173.
- [57] D. J. Schwarz, S. Hofmann, and H. Stoecker, (2001), arXiv:astro-ph/0110601.
- [58] A. M. Green, S. Hofmann, and D. J. Schwarz, JCAP **0508**, 003 (2005), arXiv:astro-ph/0503387.
- [59] T. Bringmann, New J. Phys. **11**, 105027 (2009), arXiv:0903.0189.
- [60] A. Loeb and M. Zaldarriaga, Phys. Rev. **D71**, 103520 (2005), arXiv:astro-ph/0504112.
- [61] G. Huetsi, A. Hektor, and M. Raidal, Astron. Astrophys. **505**, 999 (2009), arXiv:0906.4550.
- [62] A. W. Graham, D. Merritt, B. Moore, J. Diemand, and B. Terzic, Astron. J. **132**, 2685 (2006), arXiv:astro-ph/0509417.
- [63] A. Burkert, IAU Symp. **171**, 175 (1996), arXiv:astro-ph/9504041.
- [64] G. Bertone, D. Hooper, and J. Silk, Phys. Rept. **405**, 279 (2005), arXiv:hep-ph/0404175.
- [65] A. Bottino, F. Donato, N. Fornengo, and S. Scopel, Phys. Rev. **D68**, 043506 (2003), arXiv:hep-ph/0304080.
- [66] E. Dudas, S. Lavignac, and J. Parmentier, Nucl. Phys. **B808**, 237 (2009), arXiv:0808.0562.
- [67] E. Kuflik, A. Pierce, and K. M. Zurek, (2010), arXiv:1003.0682.
- [68] D. Das and U. Ellwanger, (2010), arXiv:1007.1151.

- [69] K. J. Bae, H. D. Kim, and S. Shin, (2010), arXiv:1005.5131.
- [70] A. Bottino, F. Donato, N. Fornengo, and S. Scopel, Phys. Rev. **D81**, 107302 (2010), arXiv:0912.4025.
- [71] D. Feldman, Z. Liu, and P. Nath, Phys. Rev. **D81**, 117701 (2010), arXiv:1003.0437.
- [72] R. Foot, Phys. Rev. **D78**, 043529 (2008), arXiv:0804.4518.
- [73] S. Chang, A. Pierce, and N. Weiner, (2008), arXiv:0808.0196.
- [74] M. Y. Khlopov, (2008), arXiv:0806.3581.
- [75] DAMA, R. Bernabei *et al.*, Mod. Phys. Lett. **A23**, 2125 (2008), arXiv:0802.4336.
- [76] E. Masso, S. Mohanty, and S. Rao, (2009), arXiv:0906.1979.
- [77] S. Chang, G. D. Kribs, D. Tucker-Smith, and N. Weiner, (2008), arXiv:0807.2250.
- [78] Y. Cui, D. E. Morrissey, D. Poland, and L. Randall, (2009), arXiv:0901.0557.
- [79] A. Bandyopadhyay, S. Chakraborty, A. Ghosal, and D. Majumdar, (2010), arXiv:003.0809.
- [80] T. Cohen, D. J. Phalen, A. Pierce, and K. M. Zurek, (2010), arXiv:1005.1655.
- [81] V. Barger, M. McCaskey, and G. Shaughnessy, (2010), arXiv:1005.3328.
- [82] Y. Farzan, S. Pascoli, and M. A. Schmidt, (2010), arXiv:1005.5323.
- [83] Y. Mambrini, (2010), arXiv:1006.3318.
- [84] J. McDonald, Phys. Rev. **D50**, 3637 (1994), arXiv:hep-ph/0702143.
- [85] C. P. Burgess, M. Pospelov, and T. ter Veldhuis, Nucl. Phys. **B619**, 709 (2001), arXiv:hep-ph/0011335.
- [86] K. Cheung, K.-H. Tsao, and T.-C. Yuan, (2010), arXiv:1003.4611.
- [87] E. Dudas, Y. Mambrini, S. Pokorski, and A. Romagnoni, JHEP **08**, 014 (2009), arXiv:0904.1745.
- [88] C. Arina, F.-S. Ling, and M. H. G. Tytgat, JCAP **0910**, 018 (2009), arXiv:0907.0430.
- [89] P. Gondolo *et al.*, JCAP **0407**, 008 (2004), arXiv:astro-ph/0406204.
- [90] G. Belanger, F. Boudjema, A. Pukhov, and A. Semenov, Comput. Phys. Commun. **176**, 367 (2007), arXiv:hep-ph/0607059.